JACS
JOURNAL OF THE AMERICAN CHEMICAL SOCIETY
Article
pubs.acs.org/JACS

Lattice Mismatch Induced Nonlinear Growth of Graphene

Ping Wu, Huijun Jiang, Wenhua Zhang, Zhenyu Li,* Zhonghuai Hou,* and Jinlong Yang

Hefei National Laboratory for Physical Sciences at Microscale, University of Science and Technology of China, Hefei, Anhui 230026, China

Supporting Information

ABSTRACT: As a two-dimensional material, graphene can be obtained via epitaxial growth on a suitable substrate. Recently, an interesting nonlinear behavior of graphene growth has been observed on some metal surfaces, but the underlying mechanism is still elusive. Taking the Ir(111) surface as an example, we perform a mechanistic study on graphene growth using a combined approach of first-principles calculations and kinetic Monte Carlo (kMC) simulations. Small carbon clusters on the terrace or at step sites are studied first. Then, we investigate how these small carbon species are attached to graphene edges. Generally, attachment of carbon atoms is thermodynamically favorable. However, due to substrate effect, there are also some edge sites where graphene growth must proceed via cluster attachment. The overall growth rate is determined by these cluster attachment processes, which have a much lower chance of happening compared to the monomer attachment. On the basis of such an inhomogeneous growth picture, kMC simulations are performed by separating different time scales, and the experimentally found quintic-like behavior is well reproduced. Different nonlinear growth behaviors are predicted for different graphene orientations, which is consistent with previous experiments. Inhomogeneity induced by lattice mismatch revealed in this study is expected to be a universal phenomenon and will play an important role in the growth of many other heteroepitaxial systems.

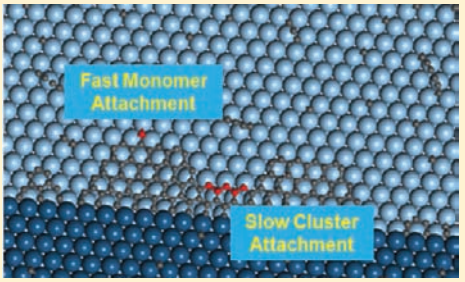

INTRODUCTION

Graphene, a monolayer of sp^2-hybridized carbon atoms, has attracted intense research interest recently due to its unique electronic structure and great application potential.[1−4] Currently, there are several ways available to produce graphene. The elegant method of micromechanical exfoliation is ready to produce high-quality samples,[1] but it is difficult to scale up. On the other hand, for solution-based mass production methods, it is still challenging to reach a high sample quality.[5] Epitaxial growth on metal surfaces can generate a large graphene sample potentially also with a high quality, which makes it the method of choice for large-scale electronic applications of graphene. Various metal surfaces (including Ni, Cu, Ru, Ir, Pd, Co, Pt, etc.) have been used to grow graphene.[6−10] Notice that, on different substrates, the graphene growth behavior can be very different.[11]

Recently, an interesting nonlinear behavior of graphene growth has been observed on Ir and some other metal surfaces.[12,13] As an attractive substrate, Ir can be used to grow large-scale graphene samples with long-range order and continuity. Graphene can spread over step edges on the Ir surface just like a carpet,[7] and it is typically well-aligned with the Ir substrate, forming moiré patterns.[14−16] These moiré patterns can then serve as templates to grow patterned structures of metal clusters, with a great potential in nanocatalysis and nanomagnetism.[17] At the same time, our previous study has shown that the Ir surface is very rigid compared to the soft Cu surface,[18,19] which makes it a good model system to study the growth mechanism of graphene.

On the Ir(111) surface, several graphene orientations have been identified.[16] Compared to the majority one (R0), three other orientations are rotated by 14° (R14), 18.5° (R18.5), and 30° (R30). This observation indicates that the interaction between graphene and the Ir substrate is not too weak to be totally orientation-independent, and it is also not too strong to only pick up a single orientation. A recent angle-resolved photoemission spectroscopy experiment suggests that graphene is chemisorbed with its R0 orientation while physisorbed with the R30 orientation.[20] Therefore, different orientations are expected to present different electronic structures, which then provides a flexibility to tune the properties of a grown graphene by controlling its orientation.[21]

Graphene growth on the Ir surface is complicated by the multiple orientational variants.[13] Typically, the R0 phase nucleates first. Then, at the boundary of a growing R0 island, one of the three minority orientations (mainly R30) can occasionally also nucleate. Once nucleated, the R30 phase grows much faster than the R0 phase. Growth kinetics of the dominant R0 phase has been carefully studied in experiment, with a nonlinear (approximately quintic to the concentration of carbon adatoms) behavior identified. This result indicates that five-membered cluster attachment plays an important role in the R0 phase growth. A homogeneous microkinetics model has been constructed to describe such a nonlinear behavior, which provides kinetic parameters via fitting experimental data.[22]

Received: February 23, 2012
Published: March 8, 2012

dx.doi.org/10.1021/ja301791x | J. Am. Chem. Soc. 2012, 134, 6045−6051

However, the homogeneity assumption adopted there has not been rationalized, and an understanding of the atomistic mechanism of graphene growth is very desirable.

In this article, first-principles calculations are carried out to study graphene growth on the Ir(111) surface. Adsorption, diffusion, and coalescence of small carbon species are considered first. Then, nucleation at step sites is discussed. Finally, the growth process is studied by attaching small carbon species to graphene edges. With all of these elementary processes understood, the overall picture of graphene growth on the Ir surface emerges, which is characterized by inhomogeneous attachment and orientation sensitivity. Since microkinetics methods based on the mean-field approximation are not expected to well describe an inhomogeneous growth,[23] a multiscale kinetic Monte Carlo (kMC) model is constructed, which well reproduces the experimentally observed nonlinear growth behavior.

COMPUTATIONAL DETAILS

First-Principles Calculations. All calculations were carried out with density functional theory implemented in the Vienna Ab Initio Simulation Package (VASP).[24,25] The Perdew−Burke−Ernzerhof (PBE) functional[26] was used to describe exchange and correlation. A 400 eV kinetic energy cutoff was chosen for plane-wave basis set, and the Monhorst-Pack *k*-point sampling[27] parameters were carefully tested to produce well-converged results. A four-layer slab model was used to describe the Ir(111) surface. The bottom layer was fixed to its bulk geometry, where the optimized Ir−Ir bond length is 2.74 Å. Repeated slabs were separated by more than 10 Å to avoid interaction between each other. Vicinal (322) and (332) surfaces were used to model the stepped Ir(111) surface, which contains {100} (A-type) and {111} (B-type) microfacets, respectively. Graphene growth front was modeled with nanoribbons. For the three minority orientations of graphene, only the R30 phase was considered since the other two are rarer than R30 by 1 order of magnitude.[16]

Potential energy of carbon clusters on Ir surface was defined as

$$E_p = (E_{C/Ir} - E_{Ir})/N_C \quad (1)$$

where $E_{C/Ir}$ and E_{Ir} are energies of the carbon cluster absorbed system and the clean Ir surface, and N_C is the number of carbon atoms in the cluster. Energy of an isolated carbon atom in a big supercell was taken as the energy reference of carbon. Climbing image nudged elastic band method[28] was used for transition state location and barrier height determination. Residual forces were within 0.02 eV/Å for both geometry optimization and transition state location.

kMC Simulations. A honeycomb lattice was adopted in kMC simulations, and its lattice sites were ready to be occupied to computationally grow graphene. Although not explicitly included, we understood that there was a hypothetical Ir substrate with a significant lattice mismatch below this honeycomb lattice, which made its lattice sites not equivalent. For simplicity, we classified all lattice sites into two types. D-type sites were those almost exactly on top of an Ir atom of the hypothetical substrate, and the rest were E-type sites (Figure S1 in the Supporting Information). The simulation box was moved forward along the growth front in the growth direction, and it was periodic in the perpendicular direction with a width of 60 sites.

In kMC simulations, the growth front was focused, where the event list was composed of attachment and detachment of various carbon species to the graphene edge. Reaction energies and barriers for these events were calculated or estimated from first-principles calculations. A multiscale algorithm was designed to overcome the huge gaps between rates of different kMC events. At each monomer concentration, the kMC simulation was performed until a statistically converged growth rate was obtained, which typically required propagation of the growth front over 10^4 sites. Finally, the least-squares method was used to fit the growth kinetics.

RESULTS AND DISCUSSION

Small Carbon Species on the Surface. Relative stabilities of different carbon species determine their evolution on the surface. In this study, as many as possible configurations of each carbon species C_N (N = 1,...,10), including both chain and compact structures, are explored (Figure S2). For a carbon monomer, the hexagonal close-packed (hcp) hollow site is the most favorable adsorption site (E_p = −7.43 eV), which is 0.26 eV more stable than the face-centered cubic (fcc) hollow site, agreeing well with previous results.[29] Carbon atom at a top site is 1.73 eV higher in energy than the hcp hollow carbon, with the underlying Ir atom pulled out from the surface by about 0.5 Å. Bridge site adsorbed carbon atom will be spontaneously relaxed to a hollow site. The subsurface octahedral site is much more unstable (1.40 eV) than the hcp hollow site, consistent with the relatively low carbon solubility in Ir.[30]

Small carbon clusters can form arching chain structures on the surface, with both their terminal carbon atoms occupying a hollow site. Alternatively, they can also form two-dimensional (2D) compact structures, which tend to be dome-like.[31] They are generally less stable than corresponding one-dimensional (1D) chain structures when their sizes are small. For clusters studied in this work, chain structure is the most stable one except for C_6 where the 2D ring structure is slightly more stable (0.06 eV/atom) than its chain structure. Notice that, with the increase of the cluster size, 2D compact structure will become more stable.[32,33]

Relative stabilities of carbon species with different sizes on the Ir(111) surface can be compared using the potential energy defined in eq 1. The result is shown in Figure 1. Carbon

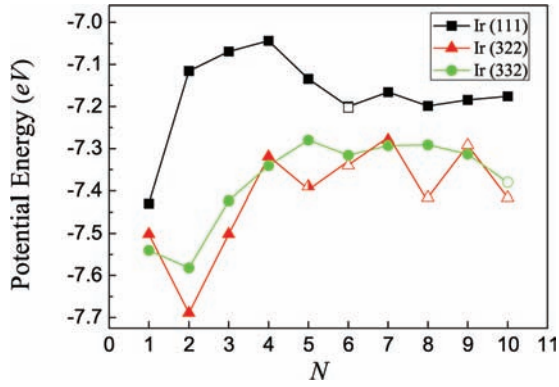

Figure 1. Potential energy (E_p) of the most stable C_N structure on the Ir(111) surface or at Ir(332) and Ir(322) steps. Hollow points mean that the most stable structure is a 2D compact structure; otherwise, it is a chain structure.

monomer is more stable than all small clusters studied in this work. Therefore, concentrations of clusters are expected to be much smaller than that of the carbon monomer on Ir(111). As a limit case, potential energy of graphene on the Ir surface is also relevant. It should be lower than that of a free-standing graphene monolayer (−7.99 eV), which is already much lower than the potential energies of the carbon species considered in this study. This is the thermodynamic driving force for graphene growth.

Mobility of small carbon species on Ir(111), which is mainly determined by the diffusion barrier, is also important for graphene growth. The diffusion barrier for a carbon monomer from hcp hollow to fcc hollow is 0.71 eV. Atom-by-atom

dx.doi.org/10.1021/ja301791x | J. Am. Chem. Soc. 2012, 134, 6045−6051

diffusion is favorable for C_2, while concerted diffusion[34] is favorable for C_3, with a diffusion barrier of 0.73 and 0.37 eV, respectively. Carbon chains can diffuse using a walk-with-legs mode (Figure S5), which leads to relatively low diffusion barriers (0.40 eV for C_5 and 0.54 eV for C_4 and C_6). When mobile carbon species meet, they can coalesce on the surface. The energy barrier for the combination of two neighboring carbon monomers is 1.44 eV, and it is similar (1.42 eV) for the incorporation of one carbon atom into an existing dimer. When adding a carbon atom to an arching chain structure of C_4, the energy barrier is decreased to 0.86 eV. Therefore, formation of small carbon clusters on the terrace is generally more difficult than their diffusion.

In graphene growth on the Ir surface, nucleation prefers to occur at step edges.[35] It is thus very desirable to study carbon species adsorption at step sites. A-type and B-type steps are considered using the (322) and (332) surfaces, respectively. By subtracting the (111) terrace contribution from the surface energy, we obtain a step formation energy of 0.37 and 0.45 eV/Å for A-type and B-type steps, respectively. We thus focus on the more stable A-type step, and the B-type will be discussed in the Supporting Information.

For A-type steps, the most stable adsorption site for atomic carbon is at their lower edge. The corresponding potential energy (E_p = −7.50 eV) is 0.07 eV lower than that of the hcp hollow carbon on the terrace, which means that the step edge is energetically more favorable than the terrace. To escape from the step edge, a 0.86 eV barrier should be conquered. A step edge fully covered with carbon monomers, however, is highly unstable (E_p = −7.00 eV). An individual dimer also tends to be attracted at step edges, with a potential energy of −7.69 eV. A step edge fully occupied by dimers has an E_p (−7.36 eV) similar to that of hcp hollow carbon. Therefore, dimers can be trapped at step edges with a relatively high concentration.

Carbon chains at the step edge can be either perpendicular to the step to form a stable handle-like structure (C5a in Figure 2)

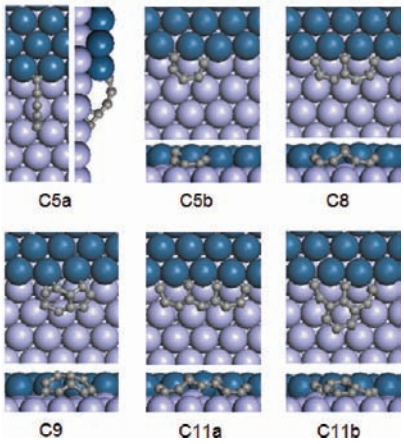

Figure 2. Carbon clusters at step sites of the Ir(322) surface.

or parallel to the step. With significant lattice mismatch, those carbon chains parallel to the step are typically not well accommodated (Figure S7). However, due to the limitation of the (322) model used for the step, we cannot study perpendicular carbon chains longer than seven. For the small cluster sizes considered here, compact structures are generally less stable than chain structures. However, a class of magic compact structures with high stabilities is still identified.

The smallest example of these magic compact structures is a C_5 cluster (C5b in Figure 2), which has the same energy as its corresponding handle-like structure (E_p = −7.39 eV). It can be considered as a structure relaxed from two dimers at the step edge connected by another carbon atom on the terrace. Since a step edge can trap many dimers, such a C_5 structure may act as a starting point of graphene growth. To check this possibility, we extend this structure to two rings (C_8). This structure is already more stable than its corresponding handle-like structure. More importantly, a fragment of the zigzag edge with the R0 orientation appears on the terrace in this structure. This is consistent with the experimental observations that the R0 phase nucleates at step edges, and it prefers to grow with zigzag edges.[35,36] Similarly, these kinds of magic structures can be further extended to three rings, either along the zigzag direction or in front of C_8 (C11a and C11b in Figure 2). Both of them have similar potential energy to that of hcp hollow carbon on the terrace. They can thus be roughly considered as crystal nucleus structures in graphene growth.

Although it is an elementary unit of graphene, a hexagon (E_p = −7.08 eV) is not as stable as the handle-like structure of C_6 at step edges. It is even less stable than a hexagon on the terrace. Therefore, graphene growth more likely starts from the semicircle C_5 structure instead of forming a hexagon at step edges. A compact 5-6 ring (C_9) becomes more stable than the corresponding chain structure along the step edge, but it is still notably less stable than its neighboring magic structures of C_8 and C_{10} (Figure S7).

Carbon Attachment at the Graphene Edge. Graphene growth kinetics is generally determined by how small carbon species are attached to edges of growing islands. Here, we use graphene nanoribbon as a model edge system. To keep the supercell reasonably small, C−C bonds are slightly stretched to match the Ir lattice. Consistent with the previous experiment about dome-like graphene islands,[31] nanoribbons also have bending edges. To study the attachment thermodynamics, we define an atom-averaged formation energy (E_f) for a specific attachment process as

$$E_f = (E_{C+R/Ir} - E_{R/Ir} - E_{C/IR} + E_{Ir})/N_C \quad (2)$$

where $E_{C+R/Ir}$ is the total energy of an absorbed ribbon with a carbon species (size N_C) attached, $E_{R/Ir}$ is the energy of the absorbed ribbon before the attachment, and $E_{C/Ir}$ is the energy of the carbon species absorbed on the surface before attachment.

For the R0 phase, we focus on the zigzag edge because it is preferred as observed in scanning tunneling microscopy and current imaging tunneling spectroscopy experiments.[35,36] Attaching a carbon monomer to a zigzag edge as shown in Figure 3a is energetically unfavorable, with an E_f equal to 0.58 eV. Since an isolated adatom is more stable, the attached carbon atom will diffuse away much faster than its attachment. Therefore, carbon monomer attachment will almost not contribute to graphene growth at such a zigzag edge. In contrary to atomic carbon, four-, five-, and six-membered carbon clusters have a driving force (about 0.36 eV) to be attached to the zigzag edge. With endothermic monomer attachment and exothermic cluster attachment, the experimentally observed nonlinear growth behavior seems to have a simple thermodynamic mechanism.

However, we also note that graphene grown on the Ir(111) surface will form a moiré structure due to lattice mismatch,[16,17] which means that different parts of graphene have different

dx.doi.org/10.1021/ja301791x | J. Am. Chem. Soc. 2012, 134, 6045−6051

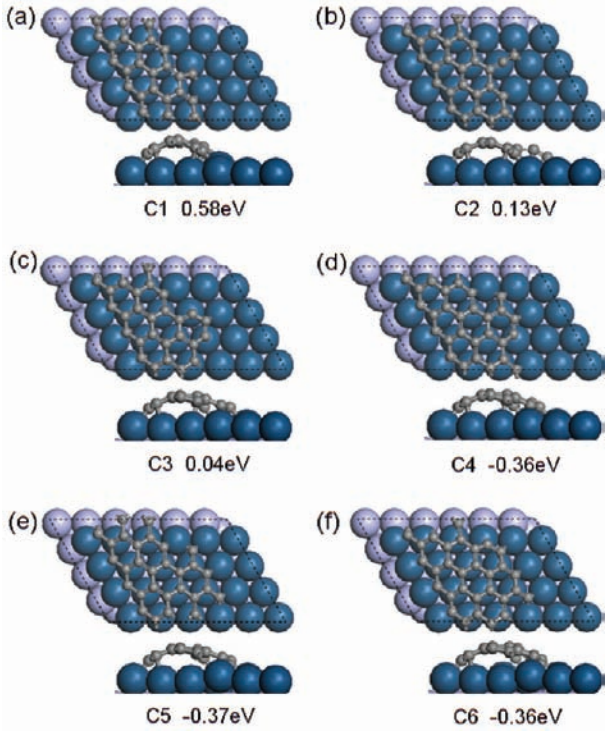

Figure 3. Optimized structure of a zigzag edge attached with different carbon clusters. E_f is marked in eV.

registries with the substrate lattice. For the R0 phase, in the atop-type region, all carbon atoms occupy hollow sites. However, in both hcp- and fcc-type regions, a hollow site carbon is immediately neighboring top site carbon atoms.[17] The model presented in Figure 3 only describes edge fragments where attached carbon atoms occupy top sites. Since top sites are energetically very unfavorable, attachment of small clusters ($N < 4$ in this case) becomes endothermic in these regions. Notice that, for monomer attachment, the attached atom in Figure 3 is not exactly at a top site. The structure with an attached atop atom (Figure 4a) is a metastable state, which leads to an E_f as high as 1.98 eV. Without taking edge bending into account, an attached carbon atom in the atop-type region is expected to occupy a hollow site instead of the top site. To describe such a behavior, we construct another ribbon model (Figure 4b). As expected, when the attached carbon atom sits at a hollow site, a different thermodynamics is obtained. The atomic carbon attachment becomes exothermic with an E_f equal to −0.86 eV.

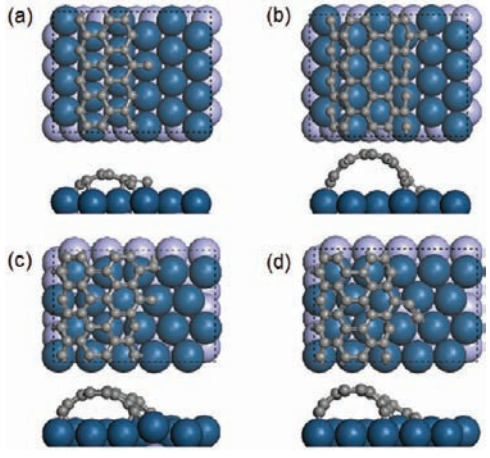

Figure 4. Optimized structure of a zigzag R0 ribbon attached with a carbon monomer occupying a (a) top or (b) hollow site. (c) Two carbon monomer and (d) a carbon dimer attached R30 zigzag edge on the Ir(111) surface.

Therefore, attachment of atomic carbon can be energetically either favorable or unfavorable depending on the growth front configuration. On the kinetic side, the energy barrier for carbon monomer attachment is 1.0 and 0.75 eV for the models in Figures 3a and 4b, respectively. These barriers are easy to be conquered at the experimental temperature. Therefore, as the most abundant species on the terrace (refer to Figure 1), carbon monomer's attachment to the graphene edge is expected to be a process with relatively great possibilities everywhere. However, for those thermodynamically unfavorable sites, its detachment will be much faster. At those sites, graphene growth relies on attachment of much rarer carbon clusters. Those parts thus grow much slower, and cluster attachment becomes the rate-determining step of graphene growth.

To further confirm the above picture with edge bending directly considered, we also perform test calculations using a large supercell (more than 205 atoms) with the period in the edge direction exactly matching the moiré pattern.[17] As shown in Figure 5, in this direction, there are 9 Ir atoms and 10 edge carbon atoms per period. In the direction perpendicular to the edge, a narrow ribbon is used. One side of the ribbon bends to the surface to mimic a growth front, while the other side of the ribbon is saturated by hydrogen atoms to mimic the interior part of a graphene island. During geometry optimization, the z coordinate of hydrogen atoms is fixed based on the experimental mean height of graphene on the Ir surface.[37] Along the zigzag edge, 8 of the 10 sites for carbon monomer attachment are energetically favorable (Figure S12). Therefore, a structure with eight carbon atoms attached and a vacancy at the two top sites (Figure 5a) can be easily formed, which is more stable (0.17 eV per attached carbon atom) than the unattached ribbon plus eight hcp hollow carbon atoms. Although the vacancy is very unfavorable for atomic carbon attachment (E_f = 2.11 eV), it is well fitted by a C_5 cluster (Figure 5b). Such a C_5 attachment process has an E_f as large as

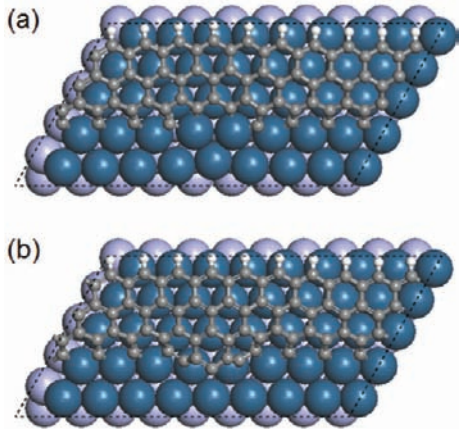

Figure 5. (a) Graphene nanoribbon with 8 of its 10 edge sites attached by carbon monomers and (b) with an additional C_5 cluster.

dx.doi.org/10.1021/ja301791x | J. Am. Chem. Soc. 2012, 134, 6045−6051

−0.70 eV. This result gives direct evidence that some parts of the graphene edge are unfavorable for atomic carbon attachment, where graphene growth proceeds only with carbon clusters provided.

Kinetic Monte Carlo Simulation. On the basis of the physical picture from first principles, we develop a kMC model to directly reproduce the experimental nonlinear growth behavior. As already pointed out by Zangwill and Vvedensky,[22] a brute-force kMC simulation will be impractical for graphene growth on Ir(111). There are mainly two difficulties. First, the growth front keeps moving, which requires a huge unit cell to get a statistically reliable growth rate. Another problem is the disparate rates of different kMC events, due to the large density differences for different surface species. For example, the gap between densities of carbon monomer and C_5 is about 10^{15}, which stretches the limit of even the most efficient algorithms for a direct simulation. To overcome these difficulties, we build a multiscale growth-front-focused kMC model.

Our kMC model is based on a honeycomb lattice, which is divided into four regions: graphene region, growth front, diffusion layer, and far field (Figure 6a). In the far field, we have a quasi-equilibrium homogeneous system of various N-sized ($N \leq 6$) carbon species. Their densities can thus be obtained from microkinetics by considering the $NC_1 \rightleftharpoons C_N$ equilibrium[38] with carbon potential energies calculated from first principles. Combined with first-principles diffusion barriers, we can further get the flux of different carbon species across the diffusion layer to the graphene growth front. In Table 1, carbon species concentration and flux data at a monomer concentration of 0.007 ML are listed as an example. Then, we focus on the carbon species attachment and detachment at the growth front, and other processes are compacted into effective carbon species fluxes. With such a model, not only do we reduce the list of kMC events but also we are able to extend the grown graphene as long as we need without extra cost.

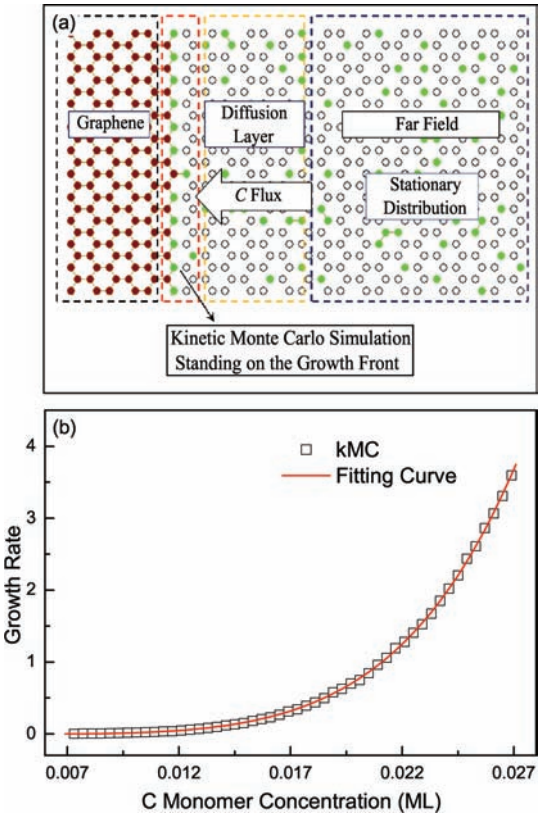

Figure 6. (a) Schematic diagram of the kMC model standing on the graphene growth front. (b) Graphene growth rates dependence on C monomer concentration obtained by kMC simulations. The solid red line is a fitted curve, and the resulting exponent is 5.25.

Due to the presence of edge heterogeneity, evolvement of the growth front should be described directly by kMC simulations.[23] Rates for the attachment and detachment of different carbon species can be calculated if kinetic data of all these events are available from first principles. Due to the effect of the Ir substrate, different sites in the honeycomb kMC lattice are generally not equivalent, which leads to a huge number of events. To build a tractable model, we make a simplification by abstracting those sites into two types. One kind of site (E-type) can be easily occupied by carbon monomers, while the others (D-type) are difficult for monomers. Under this approximation, all required kinetic data are calculated or estimated directly from first principles.

A kMC simulation with the efficient growth-front-focused model described above is still prohibited by the huge gaps between fluxes of different carbon species, as shown in Table 1. To solve this problem, we design a multiscale kMC algorithm similar to the nested stochastic simulation algorithm for chemical kinetic systems with disparate rates.[39] In our algorithm, the kMC events are grouped by the fluxes of the relevant carbon species. Events in different groups represent the evolvement of the graphene front at different time scales. For example, attachment of C monomers represents the fastest time scale. The multiscale kMC simulation is run in the following way:

(1) run a standard "event-list" kMC algorithm with all events included.

(2) once the graphene front gets stuck, which indicates that the events in the present time scale do not contribute to the graphene growth anymore, turn the simulation to the next slower time scale by turning off the events in the present group.

(3) the simulation time scale keeps jumping until the graphene grows again.

(4) once the front of graphene moves, return to step 1.

With such a specially designed kMC algorithm, we run simulations for different C monomer concentrations. Convergence of growth rate is carefully tested. The obtained relation between growth rate (r) and carbon monomer concentration (m) is fitted by $r = am^b + c$. As shown in Figure 6b, the grow rate can be perfectly described by the above equation with a b value of 5.25, which agrees with the

Table 1. Concentrations (in ML) and Fluxes (in Arbitrary Unit) of Different Carbon Species at a Carbon Monomer Concentration of 0.007 ML

	C_1	C_2	C_3	C_4	C_5	C_6
concentration	0.007	1.05×10^{-7}	7.64×10^{-12}	6.81×10^{-16}	9.54×10^{-18}	1.34×10^{-19}
flux	1.10×10^{-4}	1.35×10^{-9}	3.51×10^{-12}	5.80×10^{-17}	3.26×10^{-18}	1.14×10^{-20}

dx.doi.org/10.1021/ja301791x | J. Am. Chem. Soc. 2012, 134, 6045−6051

experiment very well. The constant term c is numerically introduced for a better fitting, and its value (−0.005) is indeed very small as expected. Notice that, in our kMC simulation, all parameters are calculated or estimated at atomic scale, without any fitting to macroscale experimental data. Therefore, the good agreement between experiment and kMC simulation confirms that the growth model revealed by our first-principles calculations has grasped the main physics for graphene growth on Ir(111).

Effects of the Graphene Orientation. Occasionally, a rotated R30 phase can be nucleated at the edge of a growing R0 phase. On the basis of the physical insights from the R0 phase, we can also make a prediction about the growth behavior of the R30 phase. We start from the moiré pattern of R30. It is different from that of the R0 phase, with more homogeneously distributed top sites.[16] In the R30 phase, two top sites are separated by at least two hollow or bridge sites. We have shown that growth of the R0 phase relies on large carbon clusters to find their right place where top sites aggregate. Although the moiré pattern is not exactly followed at graphene edges, the more homogeneous distribution of top sites in the R30 phase is expected possibly to remove this stringent large-cluster requirement. This will speed up the R30 phase growth compared to the R0 phase, as observed in the previous experiment.[13] It is worth mentioning that understanding the different growth behaviors for different graphene orientations will enable us to reduce domain boundary and thus improve the graphene sample quality.[21]

To further study the growth of the R30 phase, ribbon models are also constructed to describe the growth front. As shown in Figure 7, when a zigzag edge is chosen, carbon monomer attachment can be favorable in energy with a negative E_f. However, unlike the zigzag edge in the R0 phase, different edge atoms are not equivalent here. For example, as shown in Figure 4c, if the first attaching carbon atom has occupied an energetically favorable hollow site, the next one neighboring it has to occupy a top site, which leads to an E_f of 0.83 eV. Similar situation happens for armchair edges (Figure S13), where carbon monomer attachment is energetically favorable at some sites and not preferred at other sites. For the energetically favorable monomer attachment on the zigzag (armchair) edge, the energy barrier is 1.15 (0.99) eV. Therefore, at high temperatures, carbon monomers are expected to have the capability of attaching to graphene edges.

To make a prediction about the kinetics of R30 growth, attachment of carbon species with different sizes should be studied systematically. As shown in Figure 7, all clusters can be attached exothermically at some edge sites. For C_N with $N \geq 3$, these attachment configurations already have one or more top sites occupied. Therefore, C_3 can already stabilize a top site at graphene edges. The possibility of growing over the top site with even smaller C_2 is then checked. As shown in Figure 4d, C_2 attachment with a top site occupied is still energetically favorable, with a negative E_f equal to −0.26 eV. Since the C_2 flux is much larger than those of larger clusters, R30 phase growth will be determined by C_2 attachment and thus much faster than that of R0 relying on larger clusters. We predict that the R30 phase growth will be more or less quadratic-like instead of quintic for the R0 phase.

CONCLUSION

Atomistic details of graphene growth on the Ir(111) surface have been revealed by first-principles calculations. As building blocks of graphene, small carbon clusters have been considered first. Arching chain structures are energetically favorable on terraces, and they are also of relatively high mobilities. Magic compact structures have been identified at step edges, which are relevant to the nucleation process. Graphene nanoribbons have been used as models of the growth front. For the majority R0 orientation, the growth has been found to be quite inhomogeneous due to the lattice mismatch. At some parts of the graphene edge, atomic carbon attachment is thermodynamically prohibited, and cluster (size around 5) attachment is required. The experimentally observed nonlinear relationship between the growth rate and the carbon monomer concentration is determined by such cluster attachment steps. A delicate kMC model has been constructed to directly reproduce the experimental growth kinetics. As another result of the lattice mismatch, graphene growth on Ir(111) is sensitive to the graphene orientation. The rotated R30 phase has less inhomogeneity, which leads to a faster growth rate. A quadratic-like growth behavior has been predicted for the R30 phase. Atomistic mechanisms revealed here are essential for graphene growth condition optimization and sample quality improvement, and they are expected to be applied to other heteroepitaxial systems with a significant lattice mismatch.

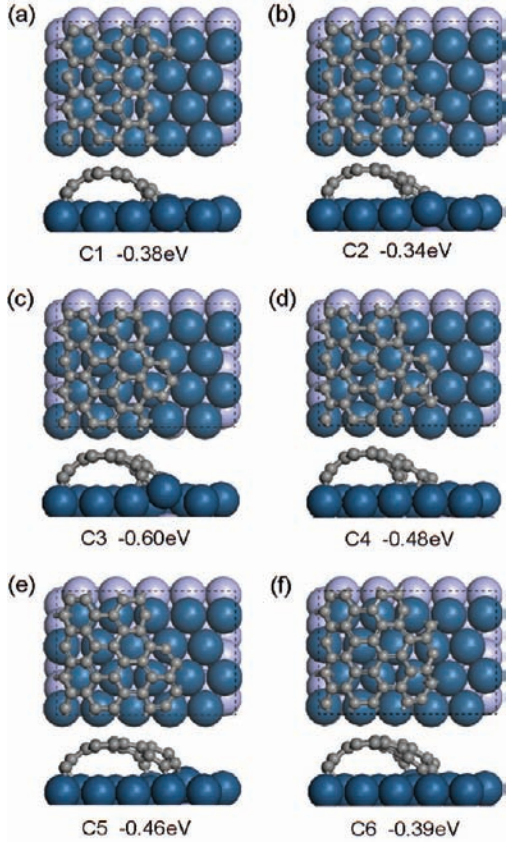

Figure 7. Optimized structure of the R30 zigzag edge attached with different carbon species on the Ir(111) surface.

ASSOCIATED CONTENT

Supporting Information

More computational details, geometry, and potential energy of small carbon species on Ir(111), Ir(322), and Ir(332), reaction paths of carbon species diffusion and coalescence, cluster attachment for armchair edges, and energy barriers for carbon

dx.doi.org/10.1021/ja301791x | J. Am. Chem. Soc. 2012, 134, 6045−6051

atom and clusters attachment. This material is available free of charge via the Internet at http://pubs.acs.org.

AUTHOR INFORMATION

Corresponding Author

zyli@ustc.edu.cn; hzhlj@ustc.edu.cn

Notes

The authors declare no competing financial interest.

ACKNOWLEDGMENTS

We are grateful to Prof. Zhenyu Zhang for helpful discussions. This work is partially supported by MOST (2011CB921404), by NSFC (21173202, 20933006, 21121003, 91027012, and 21125313), by CUSF (WK2340000011), by CAS(KJCX2-YW-W22), and by USTC-SCC, SCCAS, and Shanghai Supercomputer Centers.

REFERENCES

(1) Novoselov, K. S.; Geim, A. K.; Morozov, S. V.; Jiang, D.; Zhang, Y.; Dubonos, S. V.; Grigorieva, I. V.; Firsov, A. A. *Science* **2004**, *306*, 666.

(2) Geim, A. K. *Nat. Mater.* **2007**, *6*, 183.

(3) Geim, A. K. *Science* **2009**, *324*, 1530.

(4) Schwierz, F. *Nat. Nanotechnol.* **2010**, *5*, 487.

(5) Dreyer, D. R.; Park, S.; Bielawski, C. W.; Ruoff, R. S. *Chem. Soc. Rev.* **2010**, *39*, 228.

(6) Sutter, P. W.; Flege, J.-I.; Sutter, E. A. *Nat. Mater.* **2008**, *7*, 406.

(7) Coraux, J.; N'Diaye, A. T.; Busse, C.; Michely, T. *Nano Lett.* **2008**, *8*, 565.

(8) Li, X.; Cai, W.; An, J.; Kim, S.; Nah, J.; Yang, D.; Piner, R.; Velamakanni, A.; Jung, I.; Tutuc, E.; Banerjee, S. K.; Colombo, L.; Ruoff, R. S. *Science* **2009**, *324*, 1312.

(9) Kim, K. S.; Zhao, Y.; Jang, H.; Lee, S. Y.; Kim, J. M.; Kim, K. S.; Ahn, J.-H.; Kim, P.; Choi, J.-Y.; Hong, B. H. *Nature* **2009**, *457*, 706.

(10) Li, Z.; Wu, P.; Wang, C.; Fan, X.; Zhang, W.; Zhai, X.; Zeng, C.; Li, Z.; Yang, J.; Hou, J. *ACS Nano* **2011**, *5*, 3385.

(11) Li, X.; Cai, W.; Colombo, L.; Ruoff, R. S. *Nano Lett.* **2009**, *9*, 4268.

(12) Loginova, E.; Bartelt, N. C.; Feibelman, P. J.; McCarty, K. F. *New J. Phys.* **2008**, *10*, 093026.

(13) Loginova, E.; Bartelt, N. C.; Feibelman, P. J.; McCarty, K. F. *New J. Phys.* **2009**, *11*, 063046.

(14) N'Diaye, A. T.; Coraux, J.; Plasa, T. N.; Busse, C.; Michely, T. *New J. Phys.* **2008**, *10*, 043033.

(15) Pletikosić, I.; Kralj, M.; Pervan, P.; Brako, R.; Coraux, J.; N'Diaye, A. T.; Busse, C.; Michely, T. *Phys. Rev. Lett.* **2009**, *102*, 056808.

(16) Loginova, E.; Nie, S.; Thürmer, K.; Bartelt, N. C.; McCarty, K. F. *Phys. Rev. B* **2009**, *80*, 085430.

(17) N'Diaye, A. T.; Bleikamp, S.; Feibelman, P. J.; Michely, T. *Phys. Rev. Lett.* **2006**, *97*, 215501.

(18) Wu, P.; Zhang, W.; Li, Z.; Yang, J.; Hou, J. G. *J. Chem. Phys.* **2010**, *133*, 071101.

(19) Zhang, W.; Wu, P.; Li, Z.; Yang, J. *J. Phys. Chem. C* **2011**, *115*, 17782.

(20) Starodub, E.; Bostwick, A.; Moreschini, L.; Nie, S.; Gabaly, F. E.; McCarty, K. F.; Rotenberg, E. *Phys. Rev. B* **2011**, *83*, 125428.

(21) van Gastel, R.; N'Diaye, A. T.; Wall, D.; Coraux, J.; Busse, C.; Buckanie, N. M.; Meyer zu Heringdorf, F. J.; Horn von Hoegen, M.; Michely, T.; Poelsema, B. *Appl. Phys. Lett.* **2009**, *95*, 121901.

(22) Zangwill, A.; Vvedensky, D. D. *Nano Lett.* **2011**, *11*, 2092.

(23) Hong, Q.-J.; Liu, Z.-P. *Surf. Sci.* **2010**, *604*, 1869.

(24) Kresse, G.; Furthmüller, J. *Comput. Mater. Sci.* **1996**, *6*, 15.

(25) Kresse, G.; Furthmüller, J. *Phys. Rev. B* **1996**, *54*, 11169.

(26) Perdew, J. P.; Burke, K.; Ernzerhof, M. *Phys. Rev. Lett.* **1996**, *77*, 3865.

(27) Methfessel, M.; Paxton, A. T. *Phys. Rev. B* **1989**, *40*, 3616.

(28) Henkelman, G.; Uberuaga, B. P.; Jónsson, H. *J. Chem. Phys.* **2000**, *113*, 9901.

(29) Chen, H.; Zhu, W.; Zhang, Z. *Phys. Rev. Lett.* **2010**, *104*, 186101.

(30) Arnoult, W. J.; Mclellan, R. B. *Scr. Metall.* **1972**, *6*, 1013.

(31) Lacovig, P.; Pozzo, M.; Alfè, D.; Vilmercati, P.; Baraldi, A.; Lizzit, S. *Phys. Rev. Lett.* **2009**, *103*, 166101.

(32) Gao, J.; Yip, J.; Zhao, J.; Yakobson, B. I.; Ding, F. *J. Am. Chem. Soc.* **2011**, *133*, 5009.

(33) Van Wesep, R. G.; Chen, H.; Zhu, W.; Zhang, Z. *J. Chem. Phys.* **2011**, *134*, 171105.

(34) Yazyev, O. V.; Pasquarello, A. *Phys. Rev. Lett.* **2008**, *100*, 156102.

(35) Coraux, J.; N'Diaye, A. T.; Engler, M.; Busse, C.; Wall, D.; Buckanie, N.; Meyer zu Heringdorf, F.-J.; van Gastel, R.; Poelsema, B.; Michely, T. *New J. Phys.* **2009**, *11*, 023006.

(36) Klusek, Z.; Kozlowski, W.; Waqar, Z.; Datta, S.; Burnellgray, J.; Makarenko, I.; Gall, N.; Rutkov, E.; Tontegode, A.; Titkov, A. *Appl. Surf. Sci.* **2005**, *252*, 1221.

(37) Busse, C.; Lazić, P.; Djemour, R.; Coraux, J.; Gerber, T.; Atodiresei, N.; Caciuc, V.; Brako, R.; N'Diaye, A. T.; Blügel, S.; Zegenhagen, J.; Michely, T. *Phys. Rev. Lett.* **2011**, *107*, 036101.

(38) Kashchiev, D. *Nucleation: Basic Theory with Applications*; Butterworth-Heinemann: Oxford, 2000.

(39) E, W.; Liu, D.; Vanden-Eijnden, E. *J. Chem. Phys.* **2005**, *123*, 194107.